

Self-interacting dark matter interpretation of Crater II

Xingyu Zhang ^{1,*} Hai-Bo Yu ^{2,†} Daneng Yang ^{2,‡} and Haipeng An ^{1,3,4,§}

¹*Department of Physics, Tsinghua University, Beijing 100084, China*

²*Department of Physics and Astronomy, University of California, Riverside, California 92521, USA*

³*Center for High Energy Physics, Tsinghua University, Beijing 100084, China*

⁴*Center for High Energy Physics, Peking University, Beijing 100871, China*

(Dated: January 11, 2024)

The satellite galaxy Crater II of the Milky Way is extremely cold and exceptionally diffuse. These unusual properties are challenging to understand in the standard model of cold dark matter. We investigate the formation of Crater II in self-interacting dark matter (SIDM), where dark matter particles can scatter and thermalize. We conduct a series of controlled N-body simulations to model the tidal evolution of Crater II, varying the self-interacting cross section, orbit parameters, and initial stellar distribution. Dark matter self-interactions lead to halo core formation and the distribution of stars expands accordingly. A cored SIDM halo also boosts tidal mass loss, allowing for a high orbit. Our simulations show that SIDM halos with a 1 kpc core can simultaneously explain the low stellar velocity dispersion and the large half-light radius of Crater II, remaining robust to the initial distribution of stars. For the orbit motivated by the measurements from *Gaia* Early Data Release 3, the favored self-interacting cross section is approximately $60 \text{ cm}^2/\text{g}$ on the mass scale of Crater II.

I. INTRODUCTION

Over the past decade, astronomical surveys have discovered more than 30 satellite dwarf galaxies associated with the Milky Way, see, e.g., [1]. Among them, Crater II, located 117 kpc away from the Sun, is particularly interesting, as it has the coldest velocity dispersion of $\sigma_{\text{los}} \approx 2.7 \text{ km/s}$, while being exceptionally diffuse, with a projected half-light radius of $R_{1/2} \approx 1.07 \text{ kpc}$ [2–5]. Crater II has almost the lowest surface brightness among the satellites ever discovered. These unusual properties of Crater II make it an intriguing case for testing the standard model of cold dark matter (CDM).

Environmental effects can be important for the formation of Crater II. The tides from its host Milky Way can strip away the halo mass and lower the velocity dispersion accordingly. Refs. [6, 7] conducted cosmological hydrodynamical CDM simulations and argued that Crater II-like systems could form through strong tidal interactions. However, more tailored studies [8, 9] found that it is difficult to simultaneously realize both low velocity dispersion and large size of Crater II in CDM. The central cusp of a CDM halo is resilient to tidal stripping, and the tides must be sufficiently strong to explain the low velocity dispersion. Nevertheless, with such strong tides, the galaxy size would be truncated rapidly and it becomes much smaller than the observed size of Crater II; see [9] for detailed discussion.

In this work, we investigate the formation of Crater II within the scenario of self-interacting dark matter (SIDM). Dark matter self-interactions transport heat and thermalize the inner halo; see [10, 11] for reviews. For an SIDM halo in the core-expansion phase, a shallow density core forms and the stellar distribution expands accordingly. A cored halo also boosts tidal mass loss and mild tides are allowed for lowering the halo mass. We

conduct controlled N-body simulations to model the evolution of Crater II in the tidal field of the Milky Way in SIDM, as well as in CDM for comparison. We will show that in SIDM the simulated galaxies can well reproduce the unusual properties of Crater II. There is a degeneracy between the tidal orbit and the self-interacting cross section. Taking the orbital parameters from *Gaia* Early Data Release 3 [12, 13], we will show that the required self-interacting cross section is $\sim 60 \text{ cm}^2/\text{g}$ for Crater II.

The rest of the paper is organized as follows: In Sec. II, we introduce our simulation setup. In Sec. III, we discuss the properties of our simulated galaxies and compare them to the observations. We further discuss implications of our simulation results and conclude in Sec. IV.

II. SIMULATION SETUP

In this section, we introduce initial conditions for modeling Crater II in our N-body simulations, including initial halo and stellar density profiles and orbital parameters of our simulated satellite galaxies, the mass model of the Milky Way, and SIDM cross sections.

A. The dark matter halo of Crater II

We take three cases for the self-interacting cross section per particle mass: $\sigma/m = 10 \text{ cm}^2/\text{g}$ (SIDM10), $30 \text{ cm}^2/\text{g}$ (SIDM30), and $60 \text{ cm}^2/\text{g}$ (SIDM60); as well as the CDM limit for comparison. For all cases, we model the initial halo of Crater II with a Navarro-Frenk-White (NFW) profile [14]

$$\rho_{\text{DM}}(r) = \frac{\rho_s}{(r/r_s)(1+r/r_s)^2}, \quad (1)$$

where ρ_s and r_s are the scale density and radius, respectively. For CDM, SIDM10, and SIDM30, we take $\rho_s = 1.42 \times 10^7 M_\odot/\text{kpc}^3$ and $r_s = 2.06$ kpc. The maximum circular velocity of the halo is $V_{\text{max}} = 26.57$ km/s and its associated radius is $r_{\text{max}} = 4.45$ kpc. For SIDM60, $\rho_s = 1.14 \times 10^7 M_\odot/\text{kpc}^3$ and $r_s = 2.23$ kpc; $V_{\text{max}} = 25.77$ km/s and $r_{\text{max}} = 4.82$ kpc. The halo parameters are overall consistent with those in [9, 15].

There are stringent constraints on the cross section on the scale of galaxy clusters $\sigma/m \lesssim 0.1 \text{ cm}^2/\text{g}$ for $V_{\text{max}} \sim 1500$ km/s [16–19], and a realistic SIDM model must have a velocity-dependent cross section that decreases towards massive halos. Nevertheless, we can use an effective constant cross section for a given halo to accurately characterize its gravothermal evolution [20–24]. Thus the constant cross sections we take should be regarded as effective cross sections for the Crater II halo.

We use the public code **GADGET-2** [25, 26], which is implemented with an SIDM module developed and tested in [20], and the code **SpherIC** [27] to generate the initial condition. For all cases, the initial halo mass is $3.37 \times 10^9 M_\odot$ and there are 10^7 simulation particles. The particle mass is $337 M_\odot$ and the Plummer softening length is 7 pc. The resolution is high enough for the purpose of this work.

B. The stellar component of Crater II

Since Crater II is dark matter-dominated, we can assume that stars are massless tracers of the halo potential and use the technique introduced in [28] to model the stellar component. For each simulation particle, we can attach an appropriate probability to represent a star. The equilibrium distribution function of stars is [29]

$$f_\star(E) \equiv \frac{dN_\star}{d\Omega} = \frac{1}{\sqrt{8\pi^2}} \int_E^0 \frac{d^2\nu_\star}{d\Phi^2} \frac{d\Phi}{\sqrt{\Phi - E}} \quad (2)$$

where $d\Omega = d^3r d^3v$ is the differential volume of phase space, Φ the potential of the satellite halo, and ν_\star the stellar number density. It satisfies the normalization condition $\int dr 4\pi r^2 \nu_\star(r) = N_\star$ with N_\star being the total number of stars. As in [9], we use an Einasto profile [30] to model the stellar distribution of Crater II

$$\rho_E(r) = \rho_E(0) \exp \left[- \left(\frac{r}{r_E} \right)^\alpha \right], \quad (3)$$

where $\rho_E(0)$ is the central density, r_E is the scale radius, and we set the numerical factor $\alpha = 1$. For the Einasto profile, we have

$$\nu_\star(r) = \frac{N_\star}{8\pi r_E^3} e^{-r/r_E}. \quad (4)$$

For each simulation particle located at (\mathbf{r}, \mathbf{v}) in the phase space, the probability to represent a star is given by

$P(E) \propto f_\star(E)/f_{\text{DM}}(E)$, where $f_{\text{DM}}(E)$ is the distribution function of dark matter particles. It is calculated in a similar way as in Equation 2 with ν_\star being replaced by the number density profile of dark matter. We compute the probability at infall and reconstruct the stellar spatial distribution and kinematics from dark matter at later times by applying $P(E)$ as a weighting factor.

Ref. [2] originally used a Plummer profile to describe the stellar distribution and reported the 2D half-light radius as $R_{1/2} = 1.066$ kpc. Ref. [9] found that the Einasto profile in Equation 3 ($\alpha = 1$) fits the Plummer projected density profile well. In this work, we take the same approach and choose the initial Einasto scale radius to be $r_E = 0.40$ kpc, 0.73 kpc, and 1.37 kpc as in [9]. For later snapshots, we fit the stellar distribution using the Einasto profile as well, extract the corresponding r_E value, and calculate the half-light radius as $R_{1/2} \approx 2.03r_E$.

C. The Milky Way

We model the Milky Way with a static gravitational potential, which contains three components: a dark matter main halo, a stellar bulge, and stellar disks. The relevant parameters are given as follows.

- A spherical dark matter halo of an NFW profile

$$\Phi_{\text{halo}}(r) = -4\pi G \rho_s r_s^3 \frac{\ln(1 + r/r_s)}{r}, \quad (5)$$

with $\rho_s = 7.7 \times 10^6 M_\odot/\text{kpc}^3$ and $r_s = 20.2$ kpc.

- A spherical bulge of a Hernquist profile [31]

$$\Phi_{\text{bulge}}(r) = -\frac{GM_H}{a_H} \frac{1}{1 + r/a_H}, \quad (6)$$

with $M_H = 2.1 \times 10^{10} M_\odot$ and $a_H = 1.3$ kpc.

- Two axisymmetric disks of a Miyamoto-Nagai profile [32]

$$\Phi_{\text{disk}}(R, z) = -\frac{GM_d}{\left[R^2 + \left(a_d + \sqrt{z^2 + b_d^2} \right)^2 \right]^{1/2}}. \quad (7)$$

For the thin disk, we take $M_d = 5.9 \times 10^{10} M_\odot$, $a_d = 3.9$ kpc, and $b_d = 0.3$ kpc. For the thick disk $M_d = 2 \times 10^{10} M_\odot$, $a_d = 4.4$ kpc, and $b_d = 0.92$ kpc.

These parameters of the Milky Way are the same as those in [9, 29], which are motivated by the mass model in [33] with a circular velocity of 239 km/s at the solar radius $R_\odot = 8.3$ kpc. Since the main halo is treated as a static potential, we neglect the evaporation effect between the satellite halo and the main halo [34, 35]. The approximation is justified if the cross section in the main

halo ($V_{\max} \approx 250$ km/s) is below $\mathcal{O}(1)$ cm²/g. This condition can be satisfied naturally for velocity-dependent SIDM models that evade the cluster constraints, see, e.g., [36, 37] for examples.

D. Orbital parameters

Quantity	Value	Ref
D_{\odot} [kpc]	117.5 ± 1.1	[2]
v_{los} [km/s]	87.5 ± 0.4	[3]
α_{J2000} [deg]	117.3°	[2]
δ_{J2000} [deg]	-18.4°	[2]
μ_{α^*} [mas/yr]	-0.246 ± 0.052	[38]
	$-0.184 \pm 0.061 \pm 0.035$	[39]
	-0.07 ± 0.02	[13]
μ_{δ} [mas/yr]	-0.227 ± 0.026	[38]
	$-0.106 \pm 0.031 \pm 0.035$	[39]
	-0.11 ± 0.01	[13]

TABLE I. Measured orbital parameters of Crater II: the distance from the Sun D_{\odot} , line-of-sight velocity in the solar rest frame v_{los} , right ascension α_{J2000} and declination δ_{J2000} , proper motions μ_{α^*} and μ_{δ} .

In Table I, we summarize the measured orbital parameters of Crater II. Its proper motions are derived from data of the *Gaia* survey [40, 41] and there are quite large uncertainties among different analyses in the literature. We first consider three pairs of μ_{α^*} and μ_{δ} as in [9], denoted as Orbits 1, 2, and 3, resulting in three pericenter distances in our simulation setup, $r_p = 2.5, 13.8,$ and 37.7 kpc, respectively; see Table II. For Orbit 1, the pericenter in our setup is a factor of 1.7 smaller than the one in [9]. For Orbits 2 and 3, the agreement is within 10%. We further consider five more orbits, denoted as Orbits 4-8, and their pericenter distance is evenly distributed within the range spanned by Orbits 2 and 3. The proper motions of Orbit 3 are well consistent with the measured values based on *Gaia* Early Data Release 3 [13].

For Orbits 1 and 2, tidal stripping could remove sufficient mass of a CDM halo, after three and five pericenter passages, respectively [9]. However, Orbit 1 is too low for SIDM as core formation boosts tidal mass loss and a halo would be disrupted quickly. Thus we do not conduct the simulation with this orbit. For each dark matter model, we scan over Orbits 2-8 and identify the case that best matches Crater II in terms of the mass within $R_{1/2}$: CDM with Orbit 2, SIDM10 with Orbit 5, SIDM30 with Orbit 7, and SIDM60 with Orbit 3. In Table II, the † symbol denotes the best-matched case for each model.

III. RESULTS

In this section, we present the properties of our simulated galaxies and compare them with the observations

Orbit	μ_{α^*} [mas/yr]	μ_{δ} [mas/yr]	r_p [kpc]	σ/m [cm ² /g]
O1	-0.169	-0.267	2.5	None
O2	-0.102	-0.225	13.8	CDM†, 10
O3	-0.07	-0.11	37.7	CDM, 10, 30, 60†
O4	-0.097	-0.206	16.6	10, 30
O5	-0.091	-0.187	19.9	10†, 30
O6	-0.086	-0.168	23.7	10, 30
O7	-0.0807	-0.148	27.9	10, 30†
O8	-0.0753	-0.129	32.6	30

TABLE II. Orbital parameters considered for our CDM and SIDM simulations. Columns from left to right: Orbit name label, proper motions μ_{α^*} and μ_{δ} , pericenter distance, and SIDM cross section per mass. The † symbol denotes the case that best matches Crater II for each dark matter model and we will analyze its properties in detail. Note that Orbit 1 is not used in our production run, and Orbit 3 is well consistent with the measurements of *Gaia* Early Data Release 3 [13].

of Crater II.

A. Tidal evolution of the halo mass

In Figure 1 (left panel), we show the tidal evolution of the circular velocity at the half-light radius $V(R_{1/2}) = \sqrt{GM(R_{1/2})/R_{1/2}}$, a proxy for the halo mass within $r = R_{1/2} = 1.066$ kpc, for the four benchmark cases: CDM (black) and SIDM10 (blue), SIDM30 (magenta), and SIDM60 (red), corresponding to Orbits 2, 5, 7 and 3, respectively. We also include the CDM case with Orbit 3 for comparison (green). The horizontal line and shaded region denotes the measured value and its uncertainties $V(R_{1/2}) = 4.3 \pm 0.5$ km/s [3]. For our CDM case with Orbit 2, $V(R_{1/2})$ is close to the measured value after five pericenter passages. This is in good agreement with [9], further validating our implementation.

For the three SIDM benchmarks, $V(R_{1/2})$ reaches the measured value after several pericenter passages, and a larger pericenter is required as the cross section increases. For Orbit 3, which is based on the proper motions from *Gaia* Early Data Release 3 [13], the pericenter is $r_p = 37.7$ kpc and an SIDM model with $\sigma/m = 60$ km/s is needed, while it would be $V(R_{1/2}) \approx 15$ km/s for a CDM halo. If we relax constraints on the orbital parameters, a smaller cross section works as well. For $\sigma/m = 10$ km/s and 30 km/s, $r_p = 19.9$ kpc (Orbit 5) and 27.9 kpc (Orbit 7), respectively. We choose the timescale marked by the triangle symbol as the final snapshot for analyzing other properties of the simulated galaxies, at which they are well relaxed. In Appendix, we will show that our main results are robust to this choice.

Figure 1 (right panel) shows the corresponding circular velocity profiles at the final snapshot for the CDM and SIDM benchmarks, as well as the initial condition. The measurements at $r = R_{1/2}$ and $r = \frac{4}{3}R_{1/2}$ are $V(R_{1/2}) = 4.3_{-0.5}^{+0.5}$ km/s and $V(\frac{4}{3}R_{1/2}) = 4.8_{-0.5}^{+0.6}$ km/s [3], respec-

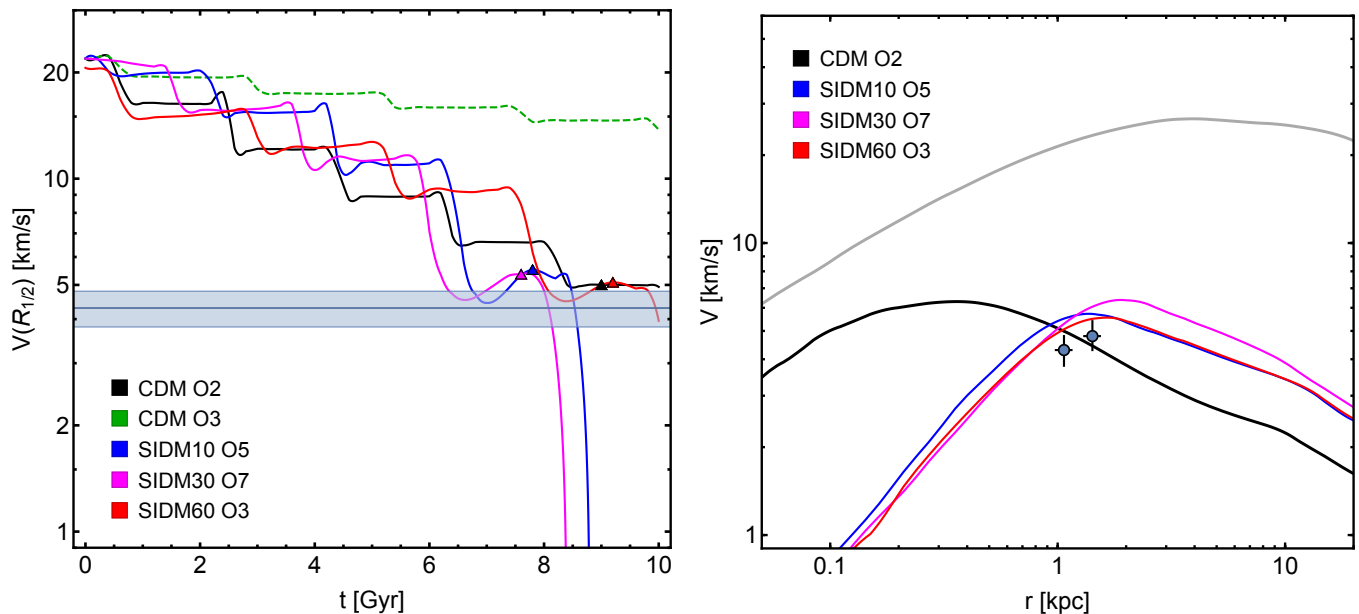


FIG. 1. Left panel: Evolution of the circular velocity at half-light radius $V(R_{1/2}) \equiv \sqrt{GM(R_{1/2})/R_{1/2}}$ for the four benchmark cases: CDM (black), SIDM $\sigma/m = 10 \text{ cm}^2/\text{g}$ (blue), $30 \text{ cm}^2/\text{g}$ (magenta), and $60 \text{ cm}^2/\text{g}$ (red), with their orbit parameters listed in Table II. For comparison, the CDM case with Orbit 2 is also shown (green). The horizontal line and shaded region denote the measured value and its uncertainties $V(R_{1/2}) = 4.3 \pm 0.5 \text{ km/s}$ [3]. The triangle symbol denotes the final snapshot for comparing the simulated galaxies with Crater II; they are relaxed after their last apocenter passage. Right panel: Corresponding circular velocity profiles of the benchmarks at the final snapshot. The gray curve denotes the initial condition. The data points with error bars represent the measurements $V(R_{1/2})$ and $V(\frac{4}{3}R_{1/2})$ from [3].

tively. Tidal stripping significantly reduces the overall halo mass, lowering the circular velocity in accord with the measurements at $r \sim R_{1/2}$ for both CDM and SIDM. However, their $V(r)$ profiles within $R_{1/2}$ are different. For the SIDM cases, $V(r)$ increases with r linearly, indicating that the SIDM halos have a shallow density core in the inner region. The halo core size is comparable to $R_{1/2} \sim 1 \text{ kpc}$. For the CDM case, $V(r)$ increases sharply from the center and then decreases as its inner halo remains cuspy even after tidal stripping.

B. The stellar distribution

We have seen that after tidal stripping both our SIDM and CDM cases can reproduce the enclosed mass within $r = R_{1/2}$ to be consistent with the measurements. Now we examine the stellar distribution of the simulated galaxies. As discussed in Section II, we used an Einasto profile in Equation 3 to model the initial stellar distribution with three values of the scale radius $r_E = 0.40 \text{ kpc}$, 0.73 kpc , and 1.37 kpc at $t = 0 \text{ Gyr}$ as in [9]. We have further checked that the Einasto profile provide an excellent fit to the stellar density profile at later times as well and determined r_E for each selected snapshot through the fit. Using the relation $R_{1/2} \approx 2.03r_E$, we convert r_E to $R_{1/2}$ and compare it to the measured value of Crater II $R_{1/2} \approx 1 \text{ kpc}$. Moreover, we compute the line-of-sight

velocity dispersion of the stellar particles.

Figure 2 shows the evolution of the half-light radius $R_{1/2}$ and the line-of-sight velocity dispersion σ_{los} of star particles within $R_{1/2}$ for the benchmarks SIDM10 (left panel), SIDM30 (middle panel), and SIDM60 (right panel), as well as the CDM case in each panel for comparison. The three initial conditions $R_{1/2} \approx 2.03r_E = 0.81 \text{ kpc}$, 1.48 kpc , and 2.78 kpc are denoted as E1 (solid; dot), E2 (dashed; square), and E3 (dotted; diamond), respectively; for each case the symbol denotes the snapshot that we conduct the evaluation. For all simulated galaxies, their size converges from the different initial values after tidal evolution. Ref. [9] shows this convergence behavior for CDM; here we find that the SIDM cases follow a similar trend, but with important distinctions.

In CDM, the galaxy size significantly reduces due to tidal truncation and all three cases with different initial $R_{1/2}$ values converge to $R_{1/2} \sim 0.3\text{--}0.4 \text{ kpc}$ at the final snapshot, too small to be consistent with the measured one $R_{1/2} \approx 1 \text{ kpc}$ [2, 3]. However, in SIDM, the size reduces mildly for the case with the largest initial $R_{1/2}$, while it actually increases for the one with the smallest initial $R_{1/2}$. Remarkably, for all SIDM benchmarks, the size converges at the final snapshot: $R_{1/2} \approx 1.1 \text{ kpc}$ for SIDM10 and SIDM60, and $R_{1/2} \approx 1.3 \text{ kpc}$ for SIDM30, in good agreement with the observed size of Crater II.

The upper limit of the galaxy size is largely set by r_{max} .

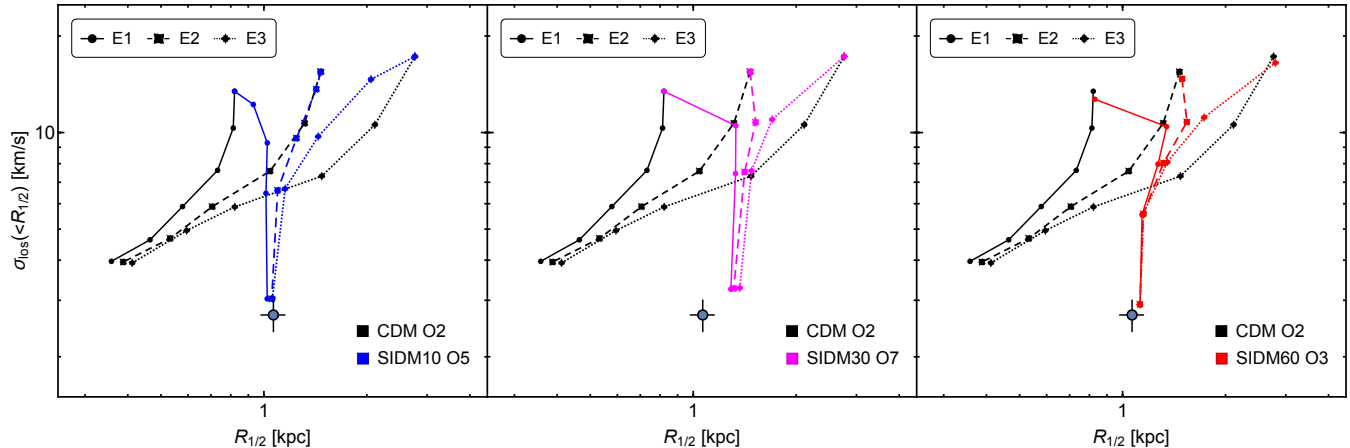


FIG. 2. The evolution of the stellar half-light radius $R_{1/2}$ and the line-of-sight velocity dispersion of stars within $R_{1/2}$ for the benchmarks: SIDM $\sigma/m = 10 \text{ cm}^2/\text{g}$ (left panel), $30 \text{ cm}^2/\text{g}$ (middle panel), and $60 \text{ cm}^2/\text{g}$ (right panel), as well as CDM in each panel for comparison. The stellar distribution follows an Einasto profile and the initial scale radii are $r_E = 0.40 \text{ kpc}$ (E1; solid), 0.73 kpc (E2; dashed), and 1.37 kpc (E3; dotted); the circle, square, and diamond symbols denote their corresponding snapshots for evaluation, respectively. The data point with error bars are from the measurements of Crater II [3].

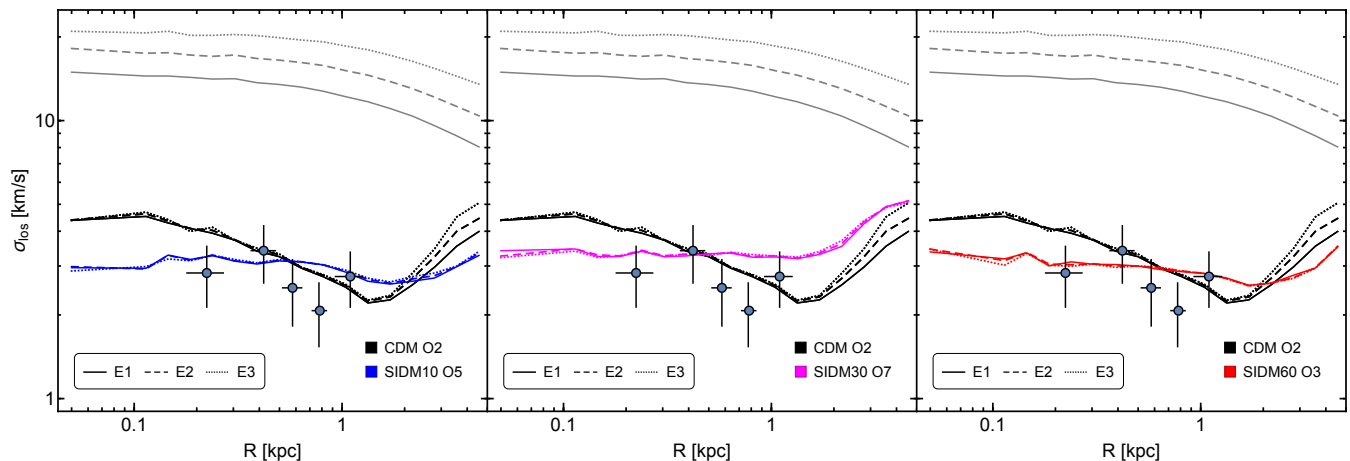


FIG. 3. The line-of-sight velocity dispersion profile of stellar particles at the initial (gray) and final (colored) snapshots for the benchmarks: SIDM $\sigma/m = 10 \text{ cm}^2/\text{g}$ (left panel), $30 \text{ cm}^2/\text{g}$ (middle panel), and $60 \text{ cm}^2/\text{g}$ (right panel), as well as CDM in each panel for comparison. The stellar distribution follows an Einasto profile and the initial scale radii are $r_E = 0.40 \text{ kpc}$ (E1; solid), 0.73 kpc (E2; dashed), and 1.37 kpc (E3; dotted). The data points with error bars are the measurements from [3].

For the region beyond r_{max} , stellar particles are stripped away significantly. From Figure. 1 (right panel), we see that $r_{\text{max}} \sim 0.4 \text{ kpc}$ for CDM, while $r_{\text{max}} \sim 1.5 \text{ kpc}$ for SIDM, at the final snapshot. Thus the latter can retain a larger galaxy size. Additionally, in SIDM the stellar distribution expands as the halo core forms [42–44]. At the final snapshot, our simulated SIDM halos have a core size of 1 kpc , which is comparable to $R_{1/2}$ of the stars.

From Figure 2, we also see that σ_{los} of the stars within $R_{1/2}$ decreases more prominent in SIDM than in CDM, although the latter has smaller pericenter. At the final

snapshot, $\sigma_{\text{los}} \approx 4 \text{ km/s}$ and 3 km/s for CDM and SIDM, respectively, and they are comparable to the measured value of Crater II $\sigma_{\text{los}} = 2.7 \pm 0.3 \text{ km/s}$ [3]. This is expected as we purposely choose orbital parameters for each case to reproduce the measured mass of Crater II within $R_{1/2}$, which is in turn estimated using the measured σ_{los} . What is remarkable is that without further adjustments SIDM can *simultaneously* predict a large galaxy size consistent with Crater II. This is not the case for CDM.

In Figure 3, we further show the line-of-sight velocity dispersion profile of stellar particles at the initial and fi-

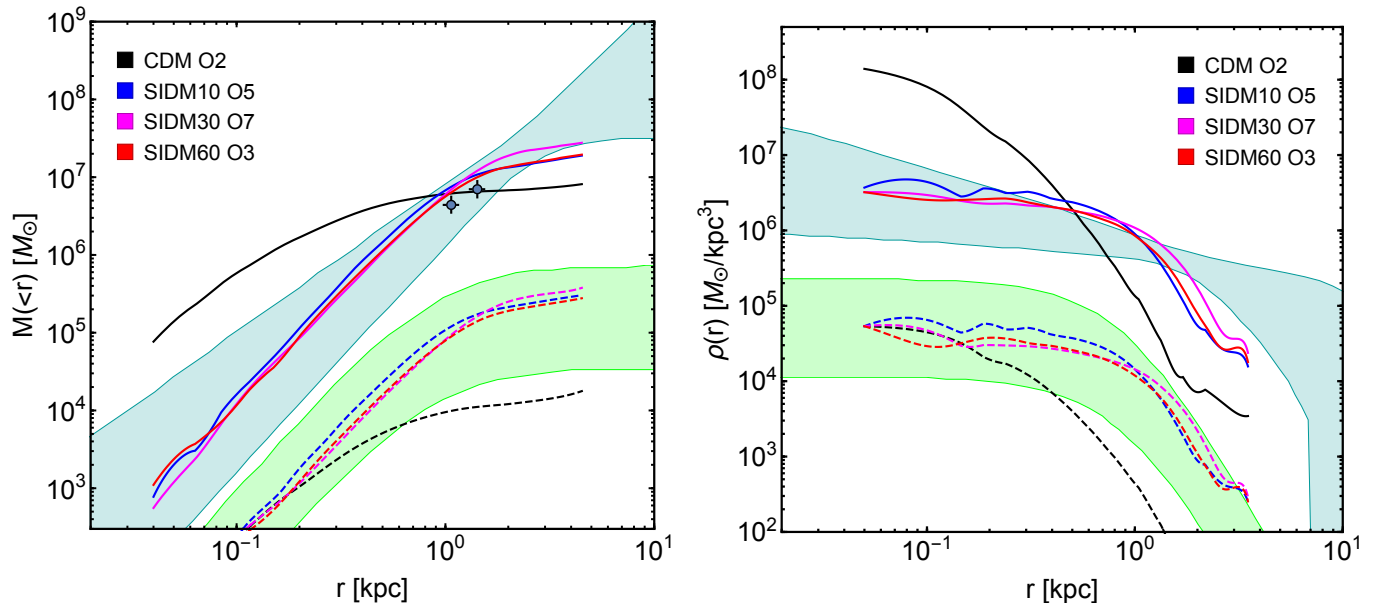


FIG. 4. Mass (left panel) and density (right panel) profiles of the dark matter (solid) and stellar (dashed) components for the CDM (black), SIDM $\sigma/m = 10 \text{ cm}^2/\text{g}$ (blue), $30 \text{ cm}^2/\text{g}$ (magenta), and $60 \text{ cm}^2/\text{g}$ (red) benchmarks at the final snapshot. The stellar density of the simulated galaxies is normalized to match the observed central stellar density of Crater II. The cyan and green bands denote the 68% credibility intervals for dark matter and stars, respectively, based on a fit to the kinematics of Crater II [3]. The data points in the left panel denote the enclosed masses evaluated within $R_{1/2}$ and $\frac{4}{3}R_{1/2}$ [3].

nal snapshots for the benchmarks SIDM10 (left panel), SIDM30 (middle panel), and SIDM60 (right panel), as well as the CDM case in each panel for comparison. Despite the difference among three σ_{los} profiles initially, they converge at their final snapshot. The velocity dispersion increases in the region for $R \gtrsim 1.5 \text{ kpc}$ as more stars are escaping at large radii. In the inner region $R \lesssim 1.5 \text{ kpc}$, the stellar dispersion profile is almost flat in SIDM as the halo has a shallow density core. In CDM, σ_{los} increases towards the center of the galaxy as expected from a central density cusp.

C. The mass and density profiles

Figure 4 shows mass (left panel) and density (right panel) profiles of the dark matter (solid) and stellar (dashed) components for our CDM and SIDM benchmarks at the final snapshot. For comparison, we also display the favored range of Crater II from [3] (cyan: halo; green: stars; 68% credibility intervals), based on the fit using a generalized NFW profile for the halo, allowing a density core. We again see that the SIDM benchmarks agree with the observations better than the CDM case. Overall, the CDM halo is too dense in the inner region, while the SIDM halos have a shallow density core with a size of $\sim 1 \text{ kpc}$, resulting in a more extended stellar distribution.

IV. DISCUSSION AND CONCLUSIONS

As we have shown, the exceptionally large size of Crater II implies that its halo has a 1 kpc density core. In CDM, a core could form due to baryonic feedback [45–49]. However, for a progenitor halo with mass $3 \times 10^9 M_{\odot}$, similar to Crater II, the FIRE2 simulation shows the core size is $\mathcal{O}(10) \text{ pc}$ [50], too small to play a role. Thus we conclude that baryonic feedback is unlikely to help reconcile CDM with the observations of Crater II.

For SIDM, there is a degeneracy between the cross section and the orbital parameters in determining the properties of satellite galaxies. Our three SIDM benchmarks are almost identical in the galaxy size and the stellar velocity dispersion at the final snapshot. To break the degeneracy, a precise determination of Crater II’s orbital parameters is needed. In fact, our Orbit 3 is based on *Gaia* Early Data Release 3 [13]. For this orbit, we found that $\sigma/m \sim 60 \text{ cm}^2/\text{g}$ at $V_{\text{max}} \sim 25 \text{ km/s}$ is needed to reproduce the observations of Crater II, while the tension with CDM becomes much more severe; see Fig. 1 (left panel; green dashed).

Our SIDM interpretation of Crater II can be extended to Antalia II, another satellite with a large size $R_{1/2} \sim 2.9 \text{ kpc}$ and $\sigma_{\text{los}} \approx 5.7 \text{ km/s}$ [51]. We expect that the self-interactions can produce a core in Antlia II. Furthermore, there are over 60 confirmed or candidate satellite galaxies of the Milky Way, see, e.g., [52, 53]. They exhibit a great diversity in both size and enclosed mass within it, with

$R_{1/2}$ ranging from ~ 10 pc to a few kpc and $V(R_{1/2}) \sim 4$ to more than 10 km/s. Thus it is intriguing to test if SIDM can explain the full range of the diversity in the $V(R_{1/2})$ – $R_{1/2}$ plane of the satellite galaxies.

Cosmological N-body simulations show that strong dark matter self-interactions can diversify inner dark matter densities of satellite halos [36, 37, 54–56], due to core formation and collapse [57, 58]. For $\sigma/m \gtrsim 30$ –50 cm^2/g in ultra-faint dwarf halos, the collapse could occur within the Hubble time, yielding a high central density. The collapse timescale is extremely sensitive to the concentration $\propto c_{200}^{-7/2}$ [37, 59–62]. The concentration of the Crater II halo is close to the median and hence it is in the core-expansion phase. Nevertheless, the dense satellites of the Milky Way, such as Draco, could be in the collapse phase [63–66]. Interestingly, $\sigma/m \sim 60$ cm^2/g on the Crater II mass scale is aligned with SIDM models proposed to explain the extreme diversity of dark matter distributions in other galactic systems, see, e.g., [36, 37].

In summary, we have performed controlled N-body simulations and shown that the unusual properties of Crater II can be explained in SIDM. Dark matter self-interactions lead to core formation and boost tidal mass loss for the satellite halo, resulting in a low velocity dispersion of stars even if the halo has a relatively large pericenter. At the same time, the stellar distribution expands as the halo core forms and the galaxy size increases accordingly. In the future, we will expand our study to other satellite galaxies of the Milky Way and explore SIDM models that can explain the full range of the diversity of the satellites.

This work of H.-B.Y. and D.Y. was supported by the John Templeton Foundation under grant ID#61884 and the U.S. Department of Energy under grant No. desc0008541. The work of H.A. was supported in part by the National Key R&D Program of China under Grants No. 2023YFA1607104, 2021YFC2203100, and 2017YFA0402204, the NSFC under Grant No. 11975134, and the Tsinghua University Dushi Program. The opinions expressed in this publication are those of the authors and do not necessarily reflect the views of the funding agencies.

APPENDIX

Figure 5 shows the $R_{1/2}$ and $\sigma_{\text{los}}(< R_{1/2})$ values for the SIDM60 benchmark with three different final snapshots denoted as t_1 , t_2 , and t_3 . In the main text, we showed the properties of the simulated galaxies at the snapshot when they are well relaxed, i.e., t_3 for SIDM60. The main results do not change if we evaluate the properties at the three different final snapshots.

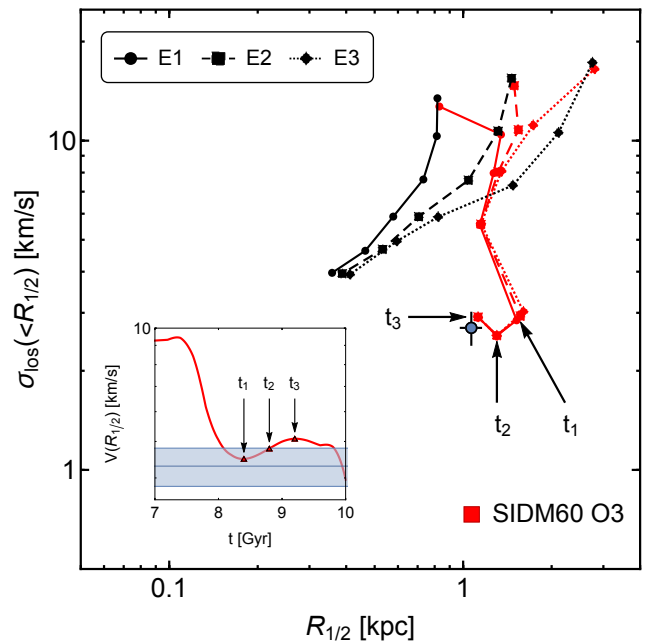


FIG. 5. Similar to the middle panel of Figure 2, but with three sequential final snapshots for the SIDM60 benchmark denoted as t_1 , t_2 , and t_3 . The insert panel shows their corresponding locations in the $V(R_{1/2})$ – t plane.

* zhang-xy19@mails.tsinghua.edu.cn

† haiboyu@ucr.edu

‡ danengy@ucr.edu

§ anhp@mail.tsinghua.edu.cn

- [1] J. D. Simon, *Ann. Rev. Astron. Astrophys.* **57**, 375 (2019), 1901.05465.
- [2] G. Torrealba, S. Koposov, V. Belokurov, and M. Irwin, *Monthly Notices of the Royal Astronomical Society* **459**, 2370 (2016).
- [3] N. Caldwell, M. G. Walker, M. Mateo, E. W. Olszewski, S. Koposov, V. Belokurov, G. Torrealba, A. Geringer-Sameth, and C. I. Johnson, *The Astrophysical Journal* **839**, 20 (2017).
- [4] S. W. Fu, J. D. Simon, and A. G. A. Jara, *The Astrophysical Journal* **883**, 11 (2019).
- [5] A. P. Ji, S. E. Koposov, T. S. Li, D. Erkal, A. B. Pace, J. D. Simon, V. Belokurov, L. R. Cullinane, G. S. Da Costa, K. Kuehn, et al., *The Astrophysical Journal* **921**, 32 (2021).
- [6] J. Frings, A. Maccio, T. Buck, C. Penzo, A. Dutton, M. Blank, and A. Obreja, *Monthly Notices of the Royal Astronomical Society* **472**, 3378 (2017).
- [7] E. Applebaum, A. M. Brooks, C. R. Christensen, F. Munshi, T. R. Quinn, S. Shen, and M. Tremmel, *The Astrophysical Journal* **906**, 96 (2021).
- [8] J. L. Sanders, N. W. Evans, and W. Dehnen, *Monthly Notices of the Royal Astronomical Society* **478**, 3879 (2018).
- [9] A. Borukhovetskaya, J. F. Navarro, R. Errani, and A. Fattahi, *Monthly Notices of the Royal Astronomical*

- Society **512**, 5247 (2022).
- [10] S. Tulin and H.-B. Yu, *Physics Reports* **730**, 1 (2018).
- [11] S. Adhikari et al. (2022), 2207.10638.
- [12] Gaia Collaboration, *Astronomy & Astrophysics* **649**, A1 (2021), 2012.01533.
- [13] A. W. McConnachie and K. A. Venn, *Research Notes of the AAS* **4**, 229 (2020).
- [14] J. F. Navarro, C. S. Frenk, and S. D. White, *The Astrophysical Journal* **490**, 493 (1997).
- [15] A. Fattahi, J. F. Navarro, C. S. Frenk, K. A. Oman, T. Sawala, and M. Schaller, *Monthly Notices of the Royal Astronomical Society* **476**, 3816 (2018).
- [16] M. Kaplinghat, S. Tulin, and H.-B. Yu, *Physical Review Letters* **116**, 041302 (2016).
- [17] D. Harvey, R. Massey, T. Kitching, A. Taylor, and E. Tittley, *Science* **347**, 1462 (2015).
- [18] L. Sagunski, S. Gad-Nasr, B. Colquhoun, A. Robertson, and S. Tulin, *Journal of Cosmology and Astroparticle Physics* **2021**, 024 (2021).
- [19] K. E. Andrade, J. Fuson, S. Gad-Nasr, D. Kong, Q. Minor, M. G. Roberts, and M. Kaplinghat, *Monthly Notices of the Royal Astronomical Society* **510**, 54 (2022).
- [20] D. Yang and H.-B. Yu, *Journal of Cosmology and Astroparticle Physics* **2022**, 077 (2022).
- [21] N. J. Outmezguine, K. K. Boddy, S. Gad-Nasr, M. Kaplinghat, and L. Sagunski, *Mon. Not. Roy. Astron. Soc.* **523**, 4786 (2023), 2204.06568.
- [22] S. Yang, X. Du, Z. C. Zeng, A. Benson, F. Jiang, E. O. Nadler, and A. H. G. Peter, *Astrophys. J.* **946**, 47 (2023), 2205.02957.
- [23] D. Yang, E. O. Nadler, H.-B. Yu, and Y.-M. Zhong (2023), 2305.16176.
- [24] M. S. Fischer, L. Kasselmann, M. Brüggen, K. Dolag, F. Kahlhoefer, A. Ragagnin, A. Robertson, and K. Schmidt-Hoberg (2023), 2310.07750.
- [25] V. Springel, N. Yoshida, and S. D. M. White, *New Astron.* **6**, 79 (2001), astro-ph/0003162.
- [26] V. Springel, *Mon. Not. Roy. Astron. Soc.* **364**, 1105 (2005), astro-ph/0505010.
- [27] S. Garrison-Kimmel, M. Rocha, M. Boylan-Kolchin, J. Bullock, and J. Lally, *Mon. Not. Roy. Astron. Soc.* **433**, 3539 (2013), 1301.3137.
- [28] J. S. Bullock and K. V. Johnston, *The Astrophysical Journal* **635**, 931 (2005).
- [29] R. Errani and J. Peñarrubia, *Monthly Notices of the Royal Astronomical Society* **491**, 4591 (2020).
- [30] J. Einasto, *Trudy Astrofizicheskogo Instituta Alma-Ata*, Vol. 5, p. 87-100, 1965 **5**, 87 (1965).
- [31] L. Hernquist, *Astrophysical Journal*, Part 1 (ISSN 0004-637X), vol. 356, June 20, 1990, p. 359-364. **356**, 359 (1990).
- [32] M. Miyamoto and R. Nagai, *Astronomical Society of Japan, Publications*, vol. 27, no. 4, 1975, p. 533-543. **27**, 533 (1975).
- [33] P. J. McMillan, *Monthly Notices of the Royal Astronomical Society* **414**, 2446 (2011).
- [34] E. O. Nadler, A. Banerjee, S. Adhikari, Y.-Y. Mao, and R. H. Wechsler, *The Astrophysical Journal* **896**, 112 (2020).
- [35] O. Slone, F. Jiang, M. Lisanti, and M. Kaplinghat, *Physical Review D* **107**, 043014 (2023).
- [36] D. Yang, E. O. Nadler, and H.-B. Yu, *The Astrophysical Journal* **949**, 67 (2023).
- [37] E. O. Nadler, D. Yang, and H.-B. Yu, *Astrophys. J. Lett.* **958**, L39 (2023), 2306.01830.
- [38] N. Kallivayalil, L. V. Sales, P. Zivick, T. K. Fritz, A. Del Pino, S. T. Sohn, G. Besla, R. P. van der Marel, J. F. Navarro, and E. Sacchi, *The Astrophysical Journal* **867**, 19 (2018).
- [39] T. Fritz, G. Battaglia, M. Pawlowski, N. Kallivayalil, R. Van Der Marel, S. Sohn, C. Brook, and G. Besla, *Astronomy & Astrophysics* **619**, A103 (2018).
- [40] A. Brown, A. Vallenari, T. Prusti, J. De Bruijne, C. Babusiaux, C. Bailer-Jones, M. Biermann, D. W. Evans, L. Eyer, F. Jansen, et al., *Astronomy & astrophysics* **616**, A1 (2018).
- [41] A. G. Brown, A. Vallenari, T. Prusti, J. De Bruijne, C. Babusiaux, M. Biermann, O. Creevey, D. Evans, L. Eyer, A. Hutton, et al., *Astronomy & Astrophysics* **649**, A1 (2021).
- [42] M. Vogelsberger, J. Zavala, C. Simpson, and A. Jenkins, *Mon. Not. Roy. Astron. Soc.* **444**, 3684 (2014), 1405.5216.
- [43] T. Carleton, R. Errani, M. Cooper, M. Kaplinghat, J. Peñarrubia, and Y. Guo, *Mon. Not. Roy. Astron. Soc.* **485**, 382 (2019), 1805.06896.
- [44] D. Yang, H.-B. Yu, and H. An, *Physical Review Letters* **125**, 111105 (2020).
- [45] J. I. Read and G. Gilmore, *Monthly Notices of the Royal Astronomical Society* **356**, 107 (2005).
- [46] S. Mashchenko, J. Wadsley, and H. Couchman, *Science* **319**, 174 (2008).
- [47] A. Pontzen and F. Governato, *Monthly Notices of the Royal Astronomical Society* **421**, 3464 (2012).
- [48] A. Di Cintio, C. B. Brook, A. V. Maccio, G. S. Stinson, A. Knebe, A. A. Dutton, and J. Wadsley, *Monthly Notices of the Royal Astronomical Society* **437**, 415 (2014).
- [49] T. Chan, D. Kereš, J. Oñorbe, P. Hopkins, A. Muratov, C.-A. Faucher-Giguere, and E. Quataert, *Monthly Notices of the Royal Astronomical Society* **454**, 2981 (2015).
- [50] A. Lazar et al., *Mon. Not. Roy. Astron. Soc.* **497**, 2393 (2020), 2004.10817.
- [51] G. Torrealba et al., *Mon. Not. Roy. Astron. Soc.* **488**, 2743 (2019), 1811.04082.
- [52] A. W. McConnachie, *The Astronomical Journal* **144**, 4 (2012).
- [53] A. Drlica-Wagner, K. Bechtol, S. Mau, M. McNanna, E. Nadler, A. Pace, T. Li, A. Pieres, E. Rozo, J. Simon, et al., *The Astrophysical Journal* **893**, 47 (2020).
- [54] J. Zavala, M. R. Lovell, M. Vogelsberger, and J. D. Burger, *Physical Review D* **100**, 063007 (2019).
- [55] H. C. Turner, M. R. Lovell, J. Zavala, and M. Vogelsberger, *Monthly Notices of the Royal Astronomical Society* **505**, 5327 (2021).
- [56] C. A. Correa, M. Schaller, S. Ploekinger, N. Anau Montel, C. Weniger, and S. Ando, *Mon. Not. Roy. Astron. Soc.* **517**, 3045 (2022), 2206.11298.
- [57] S. Balberg, S. L. Shapiro, and S. Inagaki, *The Astrophysical Journal* **568**, 475 (2002).
- [58] J. Koda and P. R. Shapiro, *Monthly Notices of the Royal Astronomical Society* **415**, 1125 (2011).
- [59] R. Essig, S. D. McDermott, H.-B. Yu, and Y.-M. Zhong, *Physical review letters* **123**, 121102 (2019).
- [60] M. Kaplinghat, M. Valli, and H.-B. Yu, *Mon. Not. Roy. Astron. Soc.* **490**, 231 (2019), 1904.04939.
- [61] Z. C. Zeng, A. H. G. Peter, X. Du, A. Benson, S. Kim, F. Jiang, F.-Y. Cyr-Racine, and M. Vogelsberger, *Mon. Not. Roy. Astron. Soc.* **513**, 4845 (2022), 2110.00259.

- [62] Z. C. Zeng, A. H. G. Peter, X. Du, S. Yang, A. Benson, F.-Y. Cyr-Racine, F. Jiang, C. Mace, and R. B. Metcalf (2023), 2310.09910.
- [63] H. Nishikawa, K. K. Boddy, and M. Kaplinghat, *Physical Review D* **101**, 063009 (2020).
- [64] O. Sameie, H.-B. Yu, L. V. Sales, M. Vogelsberger, and J. Zavala, *Phys. Rev. Lett.* **124**, 141102 (2020), 1904.07872.
- [65] F. Kahlhoefer, M. Kaplinghat, T. R. Slatyer, and C.-L. Wu, *Journal of Cosmology and Astroparticle Physics* **2019**, 010 (2019).
- [66] C. A. Correa, *Mon. Not. Roy. Astron. Soc.* **503**, 920 (2021), 2007.02958.